Computational Analysis of Turbulent Natural Convection in Water Filled Tall Enclosure

Asst. Prof. Dr.Karima E. Amori
Univ. of Baghdad/ Mech. Eng. Dept.
E-mail:drkarimaa@yahoo.com

Qasim Kadhim Hunehen
Ph.D Student, Univ. of Baghdad/ Mech. Eng. Dept.
E-mail:alqassim73@yahoo.com

ABSTRACT

In this study, the turbulent buoyancy driven fluid flow and heat transfer in a differentially heated rectangular enclosure filled with water is quantified numerically. The two dimensional governing differential equations are discretized using the finite volume method. SIMPLE algorithm is employed to obtain stabilized solution for high Rayleigh numbers by a computational code written in FORTRAN language. A parametric study is undertaken and the effect of Rayleigh numbers (10^{10} to 10^{14}), the aspect ratio (30, 40 and 50), and the tilt angle (10^{o} to 170^{o}) on fluid flow and heat transfer are investigated. The results of the adopted model in the present work is compared with previously published results and a qualitative agreement and a good validation is obtained. Results show that the fluid circulation and temperature fields are strongly affected by the enclosure tilt angle and Rayleigh Number.

KEYWORDS: Natural convection; turbulent; tall enclosure; finite volume method; heat transfer.

تحليل حسابي للحمل الحر المضطرب في حيز طويل مملوء بالماء

أ.م.د. كريمة أسماعيل عموري قاسم كاظم حنيحن

جامعة بغداد– كلية الهندسة – قسم الميكانيك

الخلاصة

تم في هذه الدراسة تقييم عددي لانتقال الحرارة وجريان المائع المضطرب والمتحرك بدافع قوة الطفو في حيز مستطيل مملوء بالماء ذو جدارين مسخنين بدرجتي حرارة مختلفتين. أعتمدت طريقة الحجوم المحددة في معالجة المعادلات التفاضلية الحاكمة ثنائية البعد. تم تطبيق منهجية SIMPLE للوصول الى حل مستقر ولقيم عدد رايلي عالية بأستخدام برنامج حسابي بلغة فورتران. اجراء دراسة لتأثير عدة متغيرات على جريان المائع وانتقال الحرارة ومن هذه المتغيرات عدد رايلي (يتراوح بين 10^{10} الى 10^{14}) ، والنسبة الباعية (30,40 و50) وزاوية ميل الحيز (من 10^{o}الى 170^{o}). بينت مقارنة نتائج النموذج العددي المتبع في هذا العمل مع تلك المنشورة في بحوث سابقة توافقاً جيداً. أظهرت النتائج أن تدوير المائع وتوزيع درجات الحرارة تتأثر كثيراً بزاوية ميل الحيز وبعدد رايلي.

الكلمات الرئيسية: حمل حر ، مضطرب، حيز طويل، طريقة الحجوم المحددة، انتقال الحرارة.

1. INTRODUCTION

Natural convection in tall enclosures with differentially heated sidewalls is importance in many engineering applications. These include energy transfer in rooms and buildings, nuclear reactor cooling, solar collectors, electronic equipment cooling, sloped or vertical double pan windows, photovoltaic-thermal systems and ventilated facades which have been frequently applied in buildings. In these cavities, the turbulent flow is completely developed, i.e., hot and cold thermal boundary layers interact and show a turbulent core and laminar sublayers near the walls, (Albet-Chico et al 2008).

Several researchers have examined the influence of the cavity inclination on the nature of the flow and convection heat transfer. (Ozoe and Sayama 1975) dealt with the problem of natural convection in inclined rectangular channels heated on one side and cooled on the opposing side. Their results indicate that minimum and maximum heat transfer occurred as inclination angle was increased from 0^o to 180^o. They found that, the angle of inclination was a strong function of the aspect ratio and a weak function of the Rayleigh number. (Elsherbiny etal.1982) examined experimentally the influence of the tilt angle and the aspect ratio of air layer on the heat transfer rate for wide range of aspect ratios, 5-110. They developed a heat transfer correlation for angle 60^o. In numerical study of (Kuyper et al. 1993) the Nusselt number shows a strong dependence on the orientation of the cavity and power law dependence on the Rayleigh number. (Lee and Lin 1995) have examined the flow structures, thermal fields, and stability conditions in vertical and inclined cubical enclosures with hot and cold side walls. This works are among the most significant treating the 3D features of the flow in closed cavities. (Elsherbiny et al. 1996) found that the average Nusselt number is decreased monotonically as the angle of tilt was increased from 0 to 180°. (Alvarado et al 2008) investigated numerically the interaction between two modes of heat transfer, natural convection and surface thermal radiation, in a tilted slender cavity of the aspect ratio ($8 \leq AR \leq 16$) and the inclination angle (15^o-35^o). Their results indicated that the coupled transport processes modifies appreciably the flow patterns and the average heat transfer in the slender cavity. The total heat transfer increases when the inclination angle increases, except when the flow structure changes from the multi-cell to the unit-cell pattern. (Cooper et al. 2009) investigated numerically and experimentally the buoyant flow in a rectangular tall cavity of 28.6 aspect ratio. They show that for moderate angles of inclination i.e. under stable temperature stratification, the main difference from the vertical case is the reduced levels of fluctuations of the velocity and temperature fields. (Cooper et al. 2012) studied experimentally the effect of inclination angle on buoyancy driven flows inside air filled tall rectangular differentially heated cavity of 28.6 aspect ratio and Rayleigh number based on temperature difference and spacing between the long sides of 0.86×10^6.

Turbulent natural convection flows in inclined, differentially heated tall cavities have received less attention than the corresponding vertical cavity flows. The objective of the present work is to study numerically the transient fluid flow and turbulent natural convection heat transfer in a tilted closed tall cavity. The momentum and energy equations are solved for turbulent flow considering natural convection between walls using finite volume technique and Low Reynolds Number LRN k-ω turbulence model of (Wilcox 1994). Parametric studies are conducted to determine the influence of each of: Rayleigh number (based on the height of cavity) with range of 10^{10} to 10^{14}, aspect ratios of 30, 40 and 50, and inclination angles of range of $10^o$to 170^o on the turbulent natural convection in tall cavity.

2. MATHEMATICAL MODEL

The geometry of interest for this study is shown in **Fig. 1**. The study is limited to two dimensional flow in a rectangular cavity of length H and width L. The two active walls, hot (x = 0) and cold (x = L), have equal dimensions and are opposite. They are maintained isothermally at high temperature T_H and low temperature T_C, respectively. The other surfaces, y=0 and y=H, are insulated. The enclosure is tilted at an angle ϕ measured from horizontal. The fluid in the cavity is assumed to be incompressible, with constant physical

properties and negligible viscous dissipation. The buoyancy effects upon momentum transfer are taken into account through the Boussinesq approximation.

For two-dimensional incompressible turbulent natural convection flow, the time-averaged governing equations, continuity, momentum and energy are:
Continuity equation:

$$\frac{\partial u}{\partial x}+\frac{\partial v}{\partial y}=0 \quad (1)$$

x and *y* momentum equations:

$$\frac{\partial u}{\partial t}+u\frac{\partial u}{\partial x}+v\frac{\partial u}{\partial y}=-\frac{1}{\rho}\frac{\partial p}{\partial x}+\frac{\partial}{\partial x}\left(\nu+\nu_t\right)\left(2\frac{\partial u}{\partial x}\right)+$$
$$\frac{\partial}{\partial y}\left(\nu+\nu_t\right)\left(\frac{\partial u}{\partial y}+\frac{\partial v}{\partial x}\right)+g\cos\phi\beta\left(T-T_o\right) \quad (2)$$
$$\frac{\partial v}{\partial t}+u\frac{\partial v}{\partial x}+v\frac{\partial v}{\partial y}=-\frac{1}{\rho}\frac{\partial p}{\partial y}+\frac{\partial}{\partial x}\left(\nu+\nu_t\right)\left(\frac{\partial v}{\partial x}+\frac{\partial u}{\partial y}\right)+$$
$$\frac{\partial}{\partial y}\left(\nu+\nu_t\right)\left(\frac{\partial v}{\partial y}\right)+g\sin\phi\beta\left(T-T_o\right) \quad (3)$$

Energy equation:

$$\frac{\partial T}{\partial t}+u\frac{\partial T}{\partial x}+v\frac{\partial T}{\partial y}=\frac{\partial}{\partial x}\left(\frac{\nu}{\mathrm{Pr}}+\frac{\nu_t}{\sigma_T}\right)\frac{\partial T}{\partial x}+$$
$$\frac{\partial}{\partial y}\left(\frac{\nu}{\mathrm{Pr}}+\frac{\nu_t}{\sigma_T}\right)\frac{\partial T}{\partial y} \quad (4)$$

The standard turbulence models like standard k-ε and standard k-ω which adopted the logarithmic wall function dose not hold near a wall for natural convection. These wall functions were originally derived for forced convection flows (Henkes et al. 1991).

A modification of standard turbulence models "the so-called Low-Reynolds Number turbulence models" were done to consider the low turbulent Reynolds number effect and the damping of the turbulence effects in the wall region. In this study LRN k-ω model by (Wilcox 1994) is employed to predict the turbulent viscosity ($\nu_t=\mu_t/\rho$) by the resolution of the turbulent kinetic energy (k) and the specific turbulent kinetic energy dissipation (ω). Hence, the additional set of equations that closes the problem is;
The turbulent kinetic energy transport equation can be written as:

$$\frac{\partial k}{\partial t}+u\frac{\partial k}{\partial x}+v\frac{\partial k}{\partial y}=\frac{\partial}{\partial x}\left(\nu+\frac{\nu_t}{\sigma_k}\right)\frac{\partial k}{\partial x}+$$
$$\frac{\partial}{\partial y}\left(\nu+\frac{\nu_t}{\sigma_k}\right)\frac{\partial k}{\partial y}+P_k+G_k-c_k f_k k\omega \quad (5)$$

The specific dissipation transport equation is defined as:

$$\frac{\partial \omega}{\partial t}+u\frac{\partial \omega}{\partial x}+v\frac{\partial \omega}{\partial y}=\frac{\partial}{\partial x}\left(\nu+\frac{\nu_t}{\sigma_\omega}\right)\frac{\partial \omega}{\partial x}+$$
$$\frac{\partial}{\partial y}\left(\nu+\frac{\nu_t}{\sigma_\omega}\right)\frac{\partial \omega}{\partial y}+c_1 f_1 P_k+c_3\frac{\omega}{k}G_k-c_2\omega^2 \quad (6)$$

The eddy viscosity is obtained from;

$$\nu_t=c_\mu f_\mu\frac{k}{\omega} \quad (7)$$

The stress production term, P_k , is modeled by:

$$P_k=\nu_t\left(2\left(\frac{\partial u}{\partial x}\right)^2+2\left(\frac{\partial v}{\partial x}\right)^2+\left(\frac{\partial u}{\partial x}+\frac{\partial v}{\partial y}\right)^2\right) \quad (8)$$

The buoyancy term, G_k, can be written as:

$$G_k=-\frac{\nu_t}{\sigma_T}g\beta\left(\cos\phi\frac{\partial T}{\partial x}+\sin\phi\frac{\partial T}{\partial y}\right) \quad (9)$$

Damping functions and constants of this turbulence model are given below, Wilcox (1994):

$$f_\mu=\frac{0.0025+R_t/6}{1+R_t/6}$$
$$f_1=\frac{0.1+R_t/2.7}{1+R_t/2.7}f_\mu^{-1}$$
$$f_k=\frac{0.278+\left(R_t/8\right)^4}{1+\left(R_t/8\right)^4}$$

$c_\mu=1$, $c_k=0.09$, $c_1=0.56$, $c_2=0.075$, $\sigma_k=2$, $\sigma_\omega=2$

c_3 is calculated as, (Henkes et al. 1991),

$$c_3 = \tanh\left|\nu/u\right|$$

where $R_t = \dfrac{k}{\omega\nu}$ is the turbulence Reynolds number.

2.1 Boundary Conditions

The fluid velocities at solid walls are equal to zero; temperatures are specified at vertical walls as ($T=T_H$ for x =0 and $T=T_C$ for x=L, ($T_C<T_H$); adiabatic conditions are given as ($\partial T/\partial y=0$ for y=0 and y=H). In the LRN k-ω turbulence model, the boundary conditions are:

k=0 at walls

and $\omega = 6\nu/\beta y_p^2$

at the first node nearest to the wall, as the value at the wall is theoretically infinity (where y_p is the normal distance of the nearest node to the wall), (Albet-Chico et al. 2008).

To obtain non-dimensional form of the governing differential equations, the following dimensionless variables are introduced:

$$X = \frac{x}{H} \quad ,Y = \frac{y}{H} \quad , \tau = \frac{t\sqrt{g\beta\Delta TH}}{H}$$

$$P = \frac{p}{\rho g\beta\Delta TH} \ ,U = \frac{u}{\sqrt{g\beta\Delta TH}} \ , V = \frac{v}{\sqrt{g\beta\Delta TH}}$$

$$\theta = \frac{T-T_C}{T_H-T_C} \ , \ k^* = \frac{k}{g\beta\Delta TH} \ , \ \omega^* = \frac{\omega H}{\sqrt{g\beta\Delta TH}}$$

The governing equations become:

Continuity equation:

$$\frac{\partial U}{\partial X} + \frac{\partial V}{\partial Y} = 0 \qquad (10)$$

Momentum equations:

$$\frac{\partial U}{\partial \tau} + U\frac{\partial U}{\partial X} + V\frac{\partial U}{\partial Y} = -\frac{\partial P}{\partial X} + \sqrt{\frac{\Pr}{Ra}}\frac{\partial}{\partial X}\left[\gamma_e\left(\frac{\partial U}{\partial X} + \frac{\partial U}{\partial Y}\right)\right]$$
$$+ \sqrt{\frac{\Pr}{Ra}}\frac{\partial}{\partial Y}\left[\gamma_e\left(\frac{\partial U}{\partial Y} + \frac{\partial V}{\partial X}\right)\right] + \theta\cos\phi \qquad (11)$$

$$\frac{\partial V}{\partial \tau} + U\frac{\partial V}{\partial X} + V\frac{\partial V}{\partial Y} = -\frac{\partial P}{\partial Y} + \sqrt{\frac{\Pr}{Ra}}\frac{\partial}{\partial X}\left[\gamma_e\left(\frac{\partial V}{\partial X} + \frac{\partial U}{\partial Y}\right)\right]$$
$$+ \sqrt{\frac{\Pr}{Ra}}\frac{\partial}{\partial Y}\left[\gamma_e\left(\frac{\partial V}{\partial Y} + \frac{\partial V}{\partial Y}\right)\right] + \theta\sin\phi \qquad (12)$$

Energy equation:

$$\frac{\partial \theta}{\partial \tau} + U\frac{\partial \theta}{\partial X} + V\frac{\partial \theta}{\partial Y} = \frac{1}{\sqrt{Ra\,\Pr}}\frac{\partial}{\partial X}\left[\left(1+\frac{\nu_t^*}{\sigma_T}\right)\frac{\partial \theta}{\partial X}\right]$$
$$+ \frac{1}{\sqrt{Ra\,\Pr}}\frac{\partial}{\partial Y}\left[\left(1+\frac{\nu_t^*}{\sigma_T}\right)\frac{\partial \theta}{\partial Y}\right] \qquad (13)$$

Normalized k-ω equations

$$\frac{\partial k^*}{\partial \tau} + U\frac{\partial k^*}{\partial X} + V\frac{\partial k^*}{\partial Y} = \sqrt{\frac{\Pr}{Ra}}\frac{\partial}{\partial X}\left[\left(1+\frac{\gamma_t^*}{\sigma_k}\right)\frac{\partial k^*}{\partial X}\right]$$
$$+ \sqrt{\frac{\Pr}{Ra}}\frac{\partial}{\partial Y}\left[\left(1+\frac{\gamma_t^*}{\sigma_k}\right)\frac{\partial k^*}{\partial Y}\right] + P_k^* + G_k^* - c_k f_k k^*\omega^* \qquad (14)$$

$$\frac{\partial \omega^*}{\partial \tau} + U\frac{\partial \omega^*}{\partial X} + V\frac{\partial \omega^*}{\partial Y} = \sqrt{\frac{\Pr}{Ra}}\frac{\partial}{\partial X}\left[\left(1+\frac{\gamma_t^*}{\sigma_\omega}\right)\frac{\partial \omega^*}{\partial X}\right]$$
$$+ \sqrt{\frac{\Pr}{Ra}}\frac{\partial}{\partial Y}\left[\left(1+\frac{\gamma_t^*}{\sigma_\omega}\right)\frac{\partial \omega^*}{\partial Y}\right] + c_1 f_1\frac{\omega^*}{k^*}P_k^* + c_3\frac{\omega^*}{k^*}G_k^*$$
$$- c_2\omega^{*2} \qquad (15)$$

where

$$Ra = \frac{\rho^2 g\beta\Delta TH^3\Pr}{\mu^2}, \quad \gamma_e = 1+\frac{\nu_t}{\nu}, \quad \gamma_t^* = \frac{\nu_t}{\nu}$$

$$P_k^* = \nu_t\sqrt{\frac{\Pr}{Ra}}\left[2\left(\frac{\partial U}{\partial X}\right)^2 + 2\left(\frac{\partial V}{\partial Y}\right)^2 + \left(\frac{\partial U}{\partial X} + \frac{\partial V}{\partial Y}\right)^2\right]$$

$$G_k^* = -\frac{1}{\sqrt{Ra\,\Pr}}\frac{\nu_t}{\sigma_T}g\beta\left(\cos\phi\frac{\partial \theta}{\partial X} + \sin\phi\frac{\partial \theta}{\partial Y}\right)$$

The dimensionless boundary conditions can be written as:

$$\theta_{(0,Y)} = 1 \ , \quad \theta_{(\frac{L}{H},Y)} = 0 \ , \quad \left(\frac{\partial \theta}{\partial Y}\right)_{Y=0} = 0 \ ,$$

$$\left(\frac{\partial \theta}{\partial Y}\right)_{Y=1} = 0 \qquad (16)$$

The normalized boundary conditions for LRN k-ω model are:
For kinetic energy $k^*=0$ at walls
and normalized specific dissipation near the wall is

$$\omega^* = \sqrt{\frac{\Pr}{Ra}}\frac{6}{\beta_o}\frac{1}{Y_p^{*2}}$$

3. NUMERICAL PROCEDURE

The general equation from which all the governing differential equations (eqs. 10 to 15) can be extracted is:

$$\frac{\partial}{\partial t}(\rho\varphi)+\frac{\partial}{\partial x_j}(\rho u_j\varphi)=\frac{\partial}{\partial x_j}\left(\Gamma\frac{\partial\varphi}{\partial x_j}\right)+S_\varphi \qquad (17)$$

The above equations have been solved using finite-volume techniques suggested by (Patankar 1980). The flow field is discretized into cells forming a staggered grid arrangement **Fig.2** and the general equation eq. (17) is converted into an algebraic equation with the following form:

$$a_P\varphi_P=\sum_{nb}a_{nb}\varphi_{nb}+a_P^o\varphi_P^o+S_u \qquad (18)$$

where 'nb' and 'o' denote the coefficient for the neighbor grids and the old time step value, respectively.

Fully implicit time integration has been applied and a pressure based method of Semi-Implicit Method for Pressure-Linked Equations (SIMPLE) is used to solve the velocity-pressure field coupling. Central differences are employed to evaluate the diffusion terms. The convective terms are discretized by means of hybrid scheme. The source terms for k and ω equations have been linearized in by adding unconditional positive values to avoid the numerical instabilities. An iterative through a line-by-line (LBL) application of the Thomas algorithm is adopted. Starting from specified initial values of the independent variables, i.e., specified initial temperature and velocity fields (as well as k and ω). Under-relaxation is introduced by means pseudo-transient for allowing and/or improving the rate of convergence.

A uniform time step and non-uniform grid has been used, with the grid clustered near walls to resolve the wall-damping effect. The spatial solution is considered to be fully converged when the maximum absolute values of both the mass source and the percent changes of the independent variables at each grid-node from iteration to iteration are smaller than a prescribed values, taken as 10^{-4}. The above solution algorithm was implemented into a computer code in FORTRAN (refer to Appendix I).

The average Nusselt number Nu_H of the hot wall is determined by:

$$Nu_H=-\int_0^1\left(\frac{\partial\theta}{\partial X}\right)_{X=0}dY \qquad (19)$$

This integral is evaluated by the trapezoidal rule.

4.VALIDATION OF THE NUMERICAL CODE

In order to validate the present numerical model, the problem of turbulent natural convection of air in a differentially heated tall cavity with an aspect ratio of 30 has been solve for Rayleigh number (based on enclosure height) of 2.43×10^{10}. A comparison of present results of vertical velocity component in the middle height of the enclosure (Y=0.5) with results of (Albets-Chico et al. 2008) for LRN k-ω , and the experimental results of (Dafa'alla and Betts 1996) is shown in **Fig.3**. A qualitative agreement and a good validation is obtained as indicated in **Table 1**. The maximum deviations obtained were of (6.5% and 4.4%) between present results and previously published data of (Albet-Chico et al. 2008) and (Dafa'Alla and Betts 1996) respectively.

Further, a mesh testing procedure was conducted to guarantee a grid independent solution. Four different mesh combinations were explored for the case of $Ra=2.43\times10^{10}$, Pr=0.7. The present code was tested for grid independence by calculating the average Nusselt number on the hot wall as shown in **Fig.4** and **Table 2**. The results confirmed that the present numerical solution is a grid independent solution and grid size of 60×180 is used in this study.

5. RESULTS AND DISCUSSION

A wide parametric numerical study was conducted for natural convection in enclosure filled with water for Rayleigh number range 10^{10} to 10^{14}, aspect ratio of (30, 40 and 50) and tilt angle range from 10^{o} to 170^{o}. The temperature difference between the hot and cold walls was fixed to 20 ^{o}C.

5.1 Vertical Velocity Component

The distributions of dimensionless vertical velocity component V with the normalized distance (i.e. X/L) along the horizontal mid-plane (i.e. Y/H= 0.5) are shown in **Fig. 5a–c** for Rayleigh number Ra=10^{12} at different values of aspect ratio AR 30, 40 and 50 respectively. The inclination angle was varied from 10^{o} to 170^{o}. There is a gradual decreasing in boundary layer thickness with increasing tilt angle ∅ from 10^{o} to 90^{o} while the velocity component V increases as shown in Fig.3a. The reverse behavior is obtained with increasing tilt angle from 90^{o} to 170^{o}.

Enclosure of aspect ratio 30 has the highest maximum velocity about active walls (for tilt angle of 100^{o}), while for aspect ratios 40 and 50 this occur approximately at the same angle with lower values. The central part of the flow between the two wall regions (or between the two velocity peaks near the hot and cold walls) shows that the mean velocity profile here crosses the zero-velocity line at a single point for the aspect ratios 40 and 50, while in the enclosure of aspect ratio 30, a no-flow core regions where the turbulence level is low have been observed as shown in Fig.3a.

The effect of Rayleigh number on the vertical velocity profile is shown in **Fig. 6a-c** for tilt angle ∅=33^{o} (which is the latitude angle in Baghdad, Iraq). **Fig. 6a-c** indicates that the magnitude of V decreases with increasing Rayleigh number Ra for a given aspect ratio. The magnitude of V decreases with aspect ratio when Rayleigh number is held constant. Moreover as Ra number increases the fluid velocity was equal to zero in the central zone of the enclosure of aspect ratio=30.

5.2 Temperature Profile

Fig. 7a-c presents the effect of the tilt angle ∅ on the temperature distribution along the horizontal mid-plane for different aspect ratios. The Rayleigh number is held at Ra=10^{12}.It is clear that the temperature distributions were nonlinear and symmetric for all the considered angles∅. These distributions essentially indicate a formation of thermal boundary layers adjacent to the hot and cold walls and an almost isothermal core at the center of the enclosure. As ∅ increases from 10^{o}, the gradients of temperature become higher close to the active walls of the cavity until ∅=95^{o} then the effect is reversed. The steepness of the temperature profile close to the vertical walls essentially determines the heat transfer rate and the maximum value of $\overline{Nu}$ is obtained for the steepest temperature gradient near-wall region. The steepness variation of the temperature profile close to the active walls decreases with increasing aspect ratio for the same Ra number as shown in **Fig. 7**.

Fig. 8 shows that as Rayleigh number increases, the temperature gradients at mid-plane increase for a given aspect ratio and inclination angle ∅. The temperature gradients decrease as aspect ratio increase. The temperature profile at Ra=10^{10} essentially indicates conduction-driven thermal transport more than convection due to smallest distance between the active walls as shown in **Fig. 8-c**.

5.3 Heat Transfer Rate

The heat transfer rate increases gradually to a maximum value at tilt angle 95^{o} and then decreases as reported in **Fig. 9**. Moreover, the average Nusselt number increases as aspect ratio increase. The variation of the average Nusselt number at enclosure hot wall for different values of aspect ratio and Rayleigh number is presented in **Fig. 10**. Higher average Nusselt number is indicated for higher aspect ratio due to the small distance between the hot and cold walls. It can also be seen that the higher heat transfer is obtained for the higher Rayleigh number. However, the average Nusselt number increases more rapidly for Ra>10^{12} due to effects of turbulent convection mode.

6. CONCLUSIONS

Turbulent natural convection in two-dimensional tall cavity has been studied numerically to examine the effect of the inclination angle and aspect ratio on the fluid

flow and heat transfer for Rayleigh numbers 10^{10}, 10^{12} and 10^{14}.

Based on the obtained results in the present study, the following conclusions can be extracted:

1. Flow and temperature fields are strongly affected by the enclosure tilt angle.
2. Rayleigh number plays an important role on thermal and fluid flow profiles.
3. The diffusion is a dominating heat transfer mechanism in tall cavity of (AR=50) at $Ra=10^{10}$ whereas at higher Rayleigh numbers ($Ra=10^{12}$ and $Ra=10^{14}$) buoyancy driven convection is dominating.
4. Maximum vertical velocity in the enclosure occurs with tilt angle of 100^{o} while maximum heat transfer rate at 95^{o} tilt angle.
5. The average Nusselt number at the heated wall does not change significantly for the diffusion dominated case whereas it increases rather rapidly with Ra for the convection dominated case.
6. Heat transfer increases with the increasing of Rayleigh, and aspect ratio can be a control parameter of heat transfer since the Nusselt number increases as the aspect ratio increases.

REFERENCES

Albet-Chico X., Oliva A., Perez-Segarra C.D., Numerical experiments in turbulent natural convection using two-equation eddy-viscosity models, J. Heat Transfer 130 (2008) 072501-11.

Alvarado R., Xamán J., Hinojosa J., Álvarez G., Interaction between natural convection and surface thermal radiation in tilted slender cavities, Int. J Thermal Sciences 47(2008) 355–368.

Cooper D., Craft T.J., Esteifi K., Iacovides H., Omranian A., The investigation of buoyant flows in differentially heated cavities, International Symposium \Turbulence Heat and Mass Transfer\ Rome 14^{th}-18^{th} Sep. 6 (2009).

Cooper D., Craft T.J., Esteifi K., Iacovides H., Experimental investigation of buoyant flows in inclined differentially heated cavities, Int. J. of Heat and Mass Transfer 55 (2012) 6321–6339.

Dafa'Alla A.A., Betts P.L., Experimental study of turbulent natural convection in a tall air cavity, Experimental Heat Transfer 9 (1996) 165-194.

ElSherbiny S.M. , Raithby G.D., Hollands K.G.T., Heat transfer by natural convection across vertical and inclined air layers, Trans ASME J. Heat Transfer 104 (1982) 96-102.

Elsherbiny S.M., Free convection in inclined air layers heated from above. Int. J Heat Mass Transfer 39 (18) (1996) 3925–30.

Henkes R.A.W.M., Van Der Vlugt F.F., Hoogendoorn C.J., Natural convection flow in a square cavity calculated with low-Reynolds-number turbulence models, Int. J. Heat Mass Transfer 34 (2) (1991) 377-388.

Kuyper R.A., Van Der Meer Th.H., Hoogendorn C.J., Henkes R.A.W., Numerical study of laminar and turbulent natural convection in an inclined square cavity, Int. J. Heat Mass Transfer 36(1993) 2899–2911.

Lee T., Lin T.F., Three dimensional natural convection of air in an inclined cubic cavity. Numerical Heat Transfer Part A 27 (1995) 681–703.

Ozoe H., Sayama H., Natural convection in an inclined rectangular channel at various aspect ratios and angles-experimental measurements, Int. J. Heat Mass Transfer 18 (1975) 1425-1431.

Patankar S.V., Numerical heat transfer and fluid flow, Hemisphere, Washington, DC (1980).

Wilcox D.C., Simulation of transition with a two-equation turbulence model, AIAA J. 32 (1994) 247-255.

Table 1 Comparison of the present results with previously published results (for air, AR=30 and Ra=2.34×10^{10})

	Nu	V_{max} (Y=H/2)	$\mu^*_{t\,max}$
Numerical [1]	133.67 (-10.2%)	-	21.83 (-28%)
Present study	142.39 (-4.4%)	0.09658 (0.95%)	22.68 (-25%)
Experimental[12]	149.0	0.09567	30.40

Table 2 Grid independence study

Grid size	Nu_{avg}
40×200	142.070
40×180	142.072
60×200	142.180
60×180	142.390

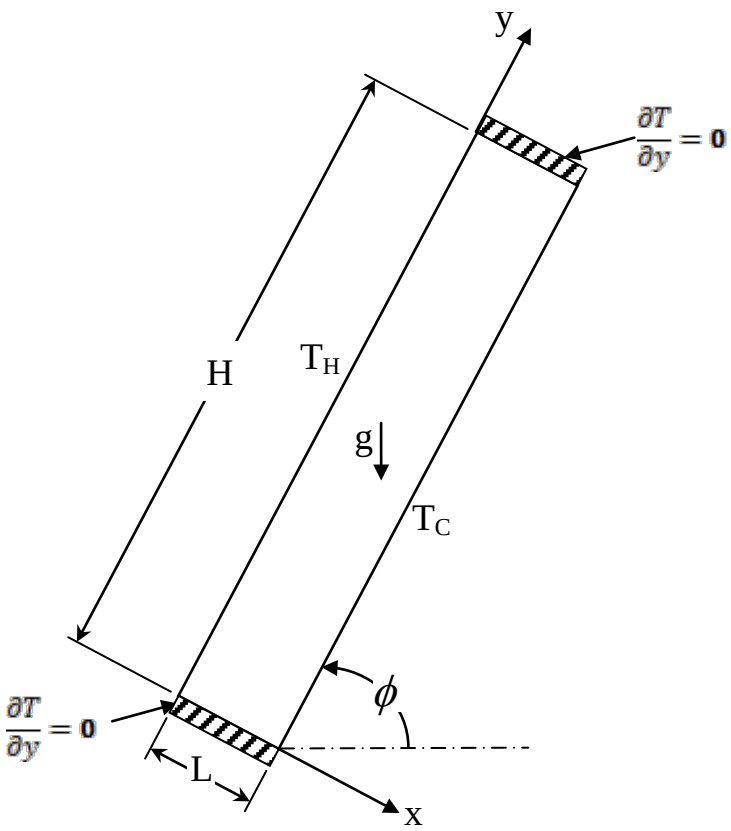

Fig.1 Schematic diagram of the enclosure configurations

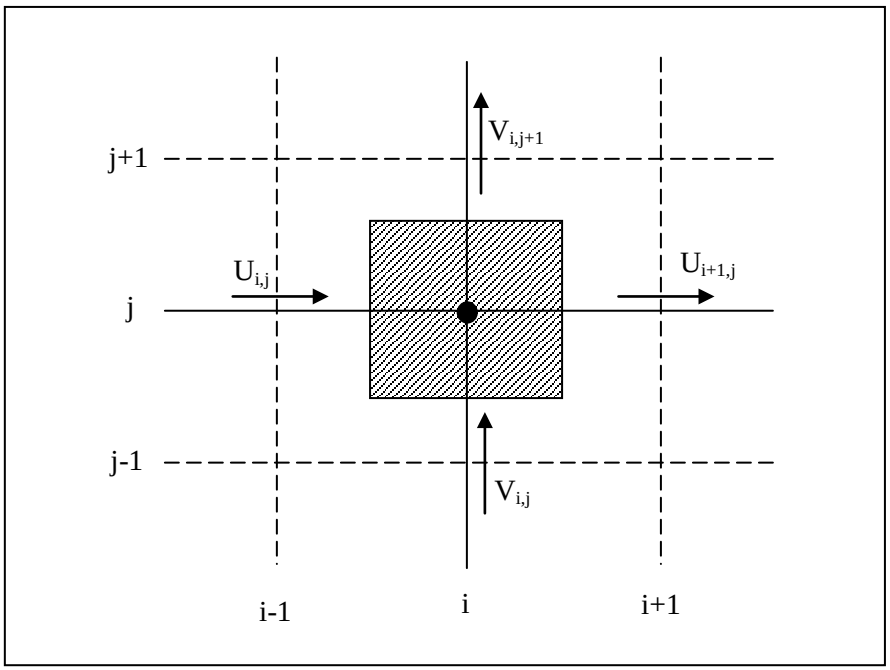

Fig. 2 A typical control volume showing the locations of the principle variables
- Scalar variables at point (i,j), $P_{i,j}$, $T_{i,j}$, $k_{i,j}$,$\omega_{i,j}$,….
- $U_{i,j}$ and $V_{i,j}$ at staggered grids.

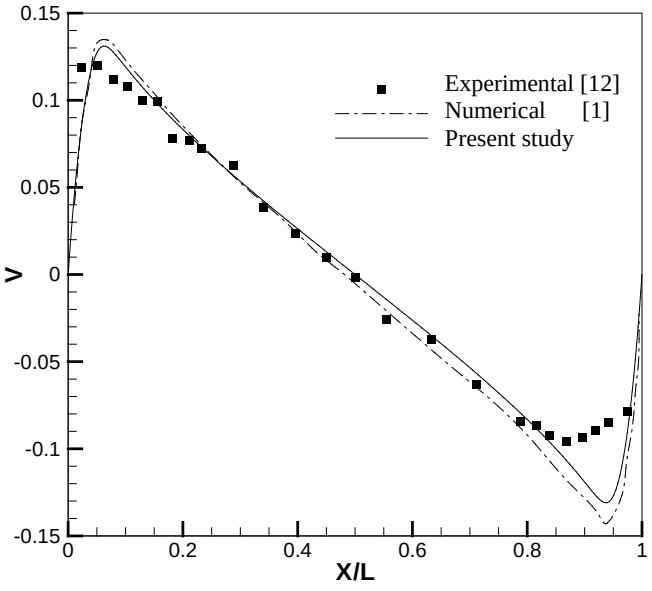

Fig.3 Comparison of vertical-velocity profiles of air at Y=0.5 in cavity of AR=30 and

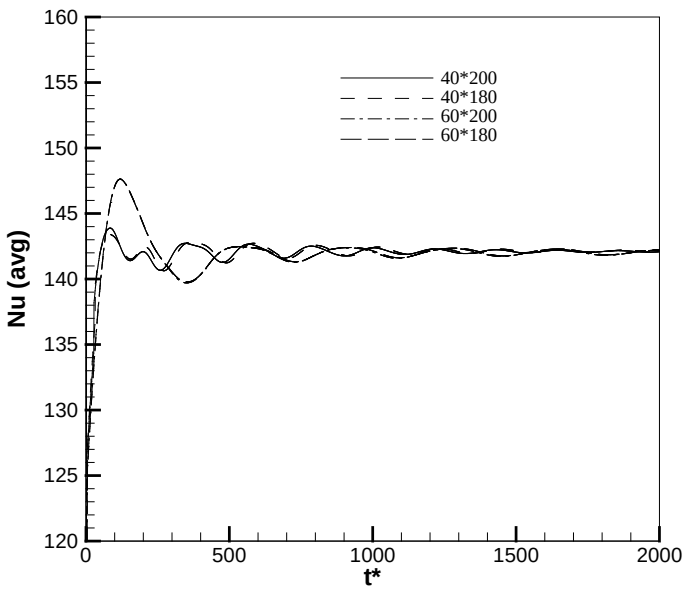

Fig. 4 Nusselt average for different grid size (AR=30 and Ra=2.43×1010)

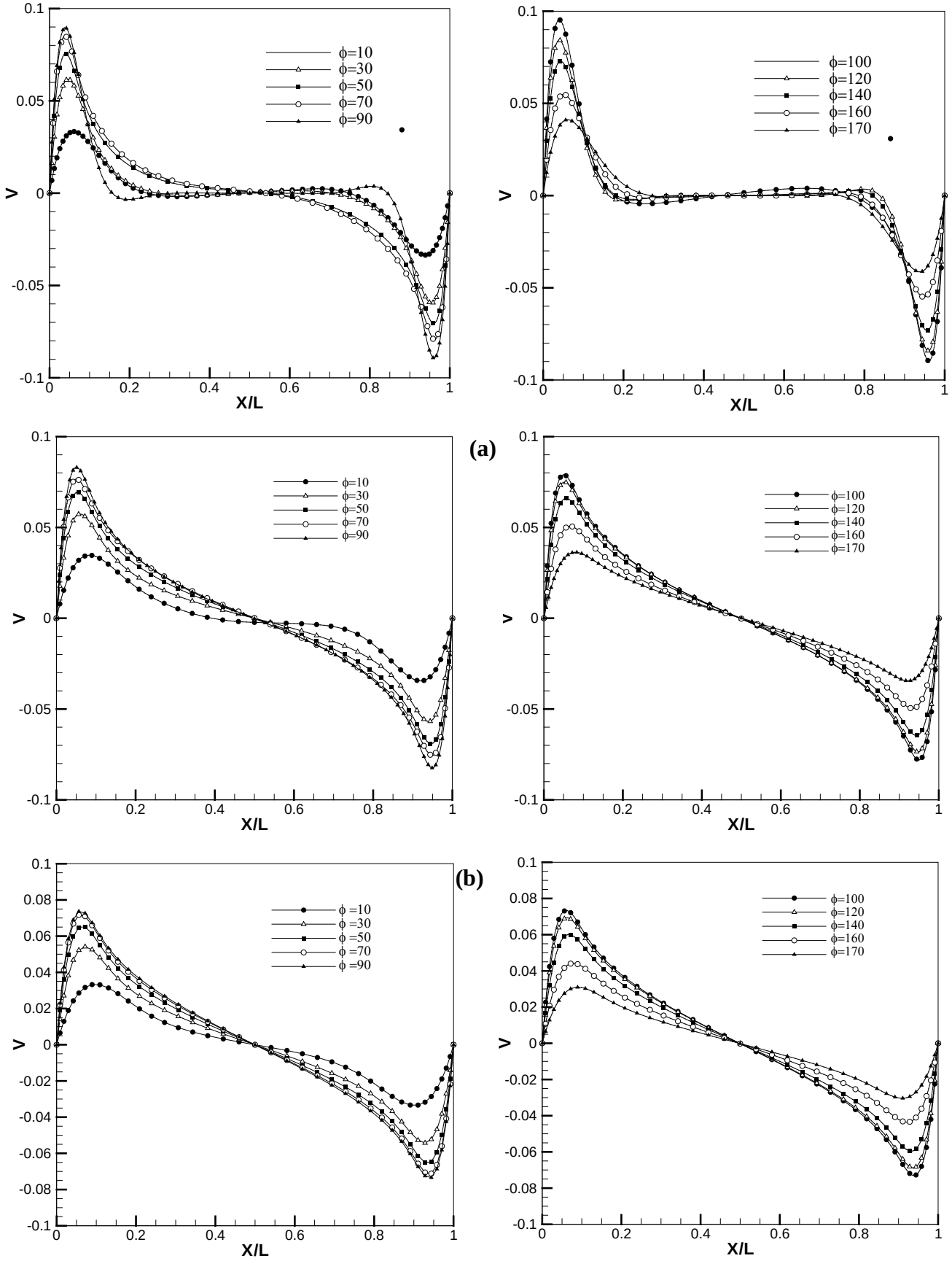

Fig.5 Variations of vertical velocity component V along the horizontal mid-plane for water (Pr=7.1), Ra=10^{12}: (a) AR=30, (b) AR=40 and (c) AR=50.

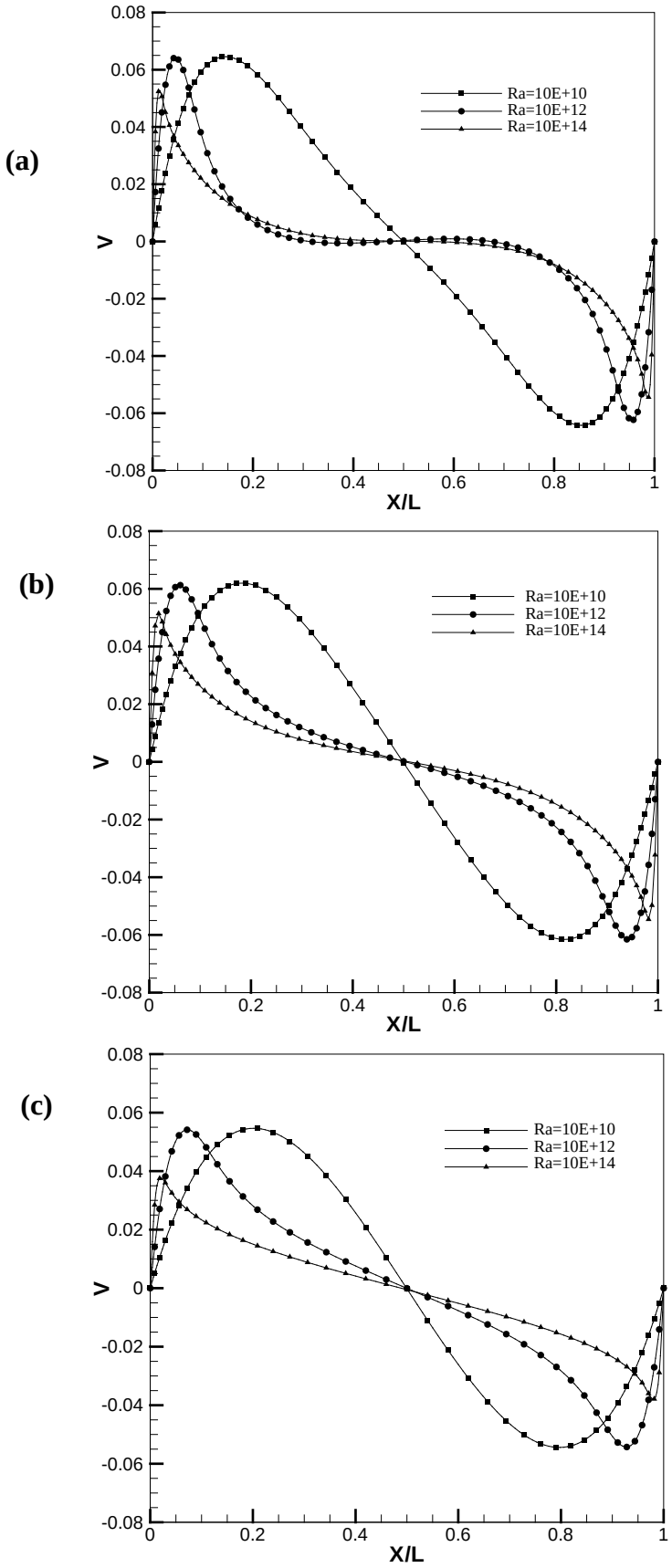

Fig.6 Variations of vertical velocity component V along the horizontal mid-plane for water (Pr=7.1), and ∅=33°: (a) AR=30, (b) AR=40 and (c) AR=50.

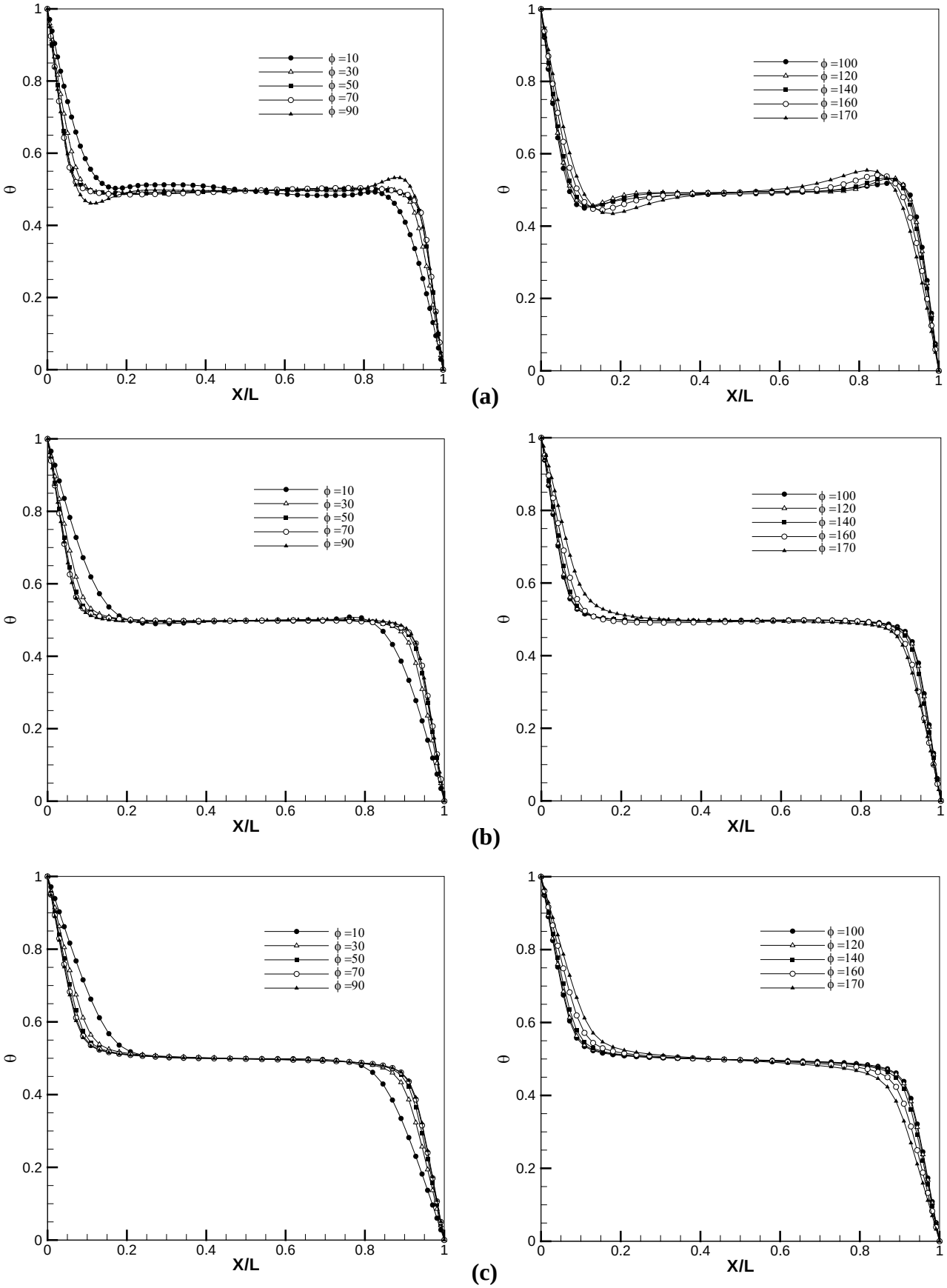

Fig.7 Temperature profiles at the horizontal mid-plane for water (Pr=7.1), and Ra=10^{12}(a) AR=30, (b) AR=40 and (c)

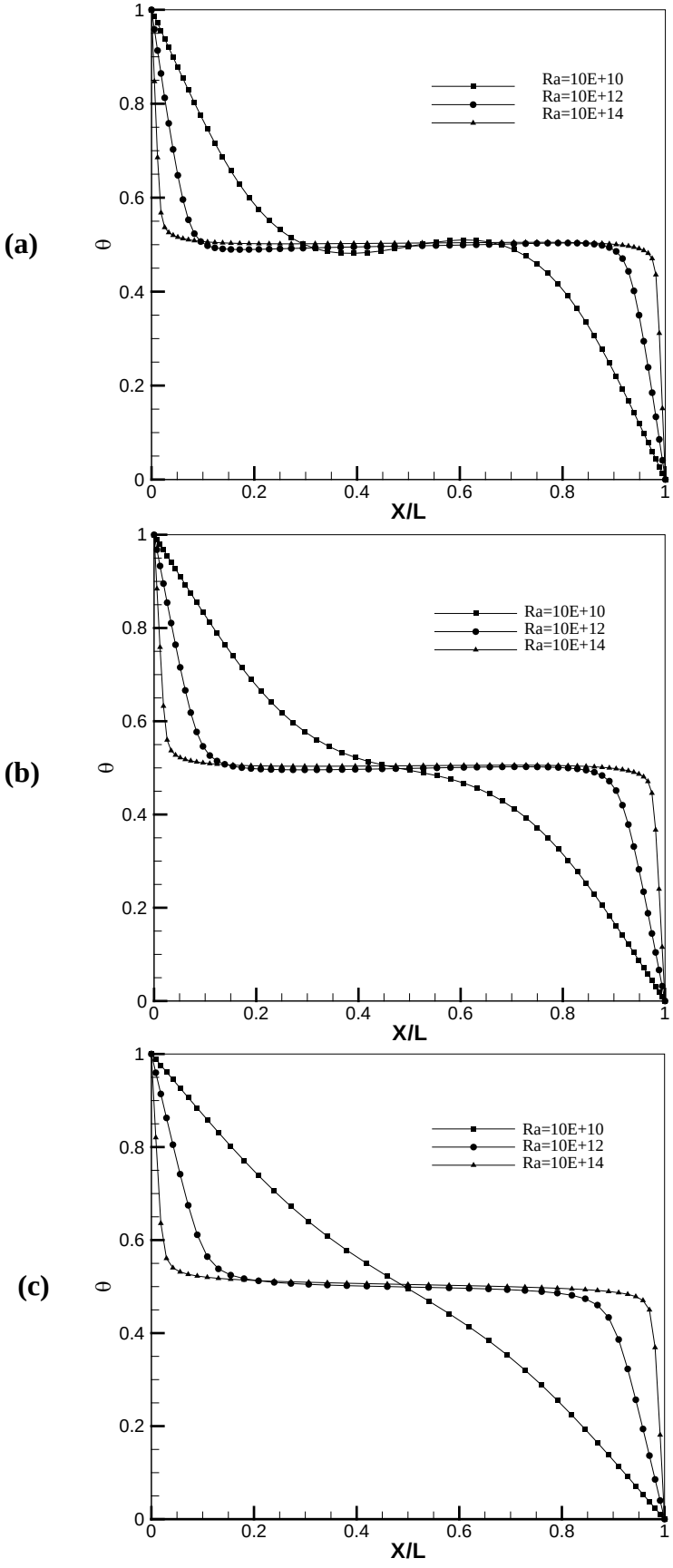

Fig.8 Temperature profiles at the horizontal mid-plane for water (Pr=7.1), and ∅=33°(a) AR=30, (b) AR=40 and (c) AR=50.

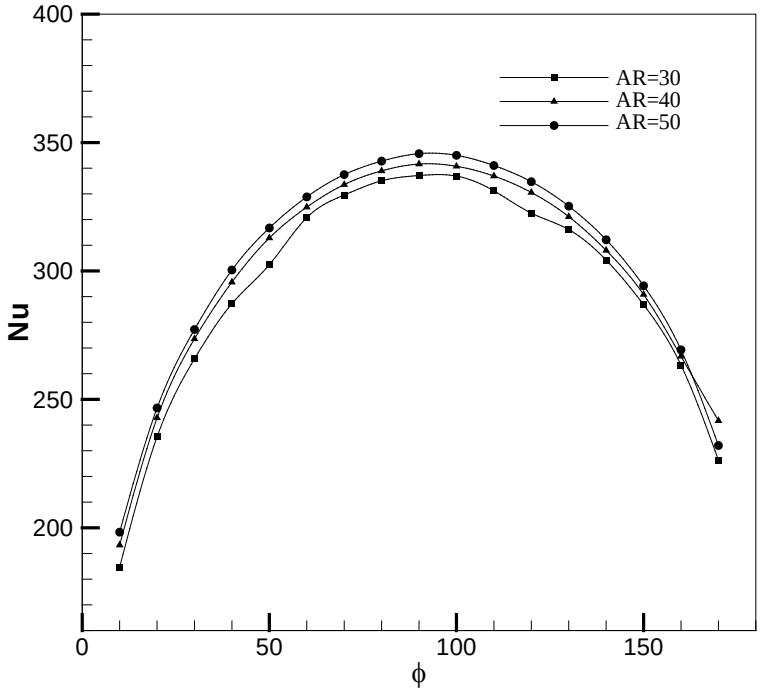

Fig.9 Variation of average Nusselt number versus tilt angle for $Ra=10^{12}$ and different aspect ratios.

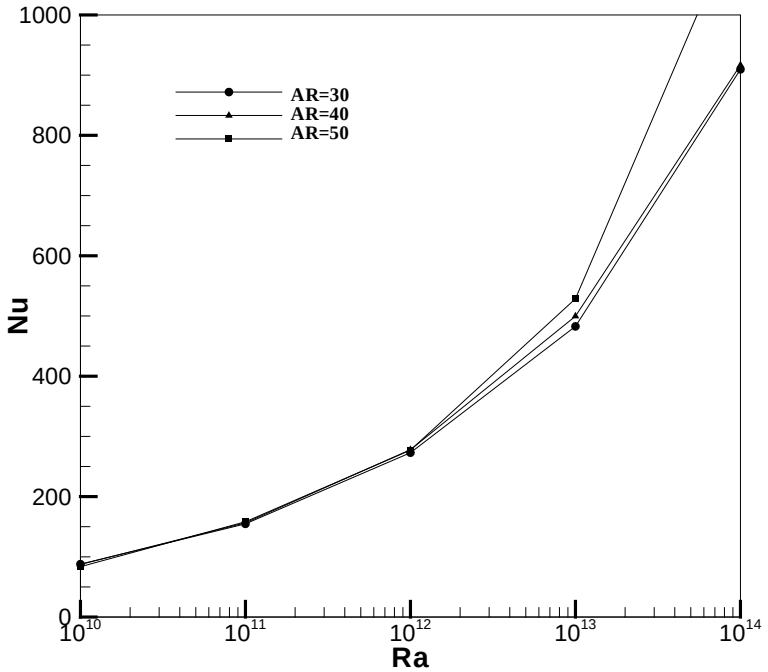

Fig.10 Average Nusselt number for turbulent natural convection for angle ∅=33°.

NOMENCLATURE

AR	Aspect Ratio =H/L
c_μ, c_1, c_2, c_3	Coefficients of turbulence model
f_1, f_2, f_μ	Damping functions of turbulence model
g_i	Gravitational acceleration (m/s^2)
G_k	Production of kinetic energy due to buoyancy effects (m^2/s^3)
H	Height of enclosure (m)
i,j	Vector direction
k	Turbulent kinetic energy (m^2/s^2)
k^*	Dimensionless turbulent kinetic energy
L	Width of enclosure (m)
Nu	Nusselt number
P_k	Production of kinetic energy due to shear stresses (m^2/s^3)
Pr	Prandtl number
P	Pressure (N/m^2)
Ra	Rayleigh number (based on height)($Ra=g\beta\Delta TH^3Pr/\nu^2$)
Rt	Turbulence Reynolds number
T	Temperature (K)
t	Time (s)
u	Velocity in x-direction (m/s)
U	Dimensionless velocity ($u/\sqrt{g\beta\Delta TH}$)
v	Velocity in y-direction (m/s)
V	Dimensionless velocity ($v/\sqrt{g\beta\Delta TH}$)
x,y	Cartesian coordinates
X,Y	Dimensionless coordinates

Greek Symbols

β	Thermal expansion coefficient (l/K)
$\emptyset$	Tilted angle (deg)
φ	Any dependent variable in numerical solution
μ	Dynamic viscosity (kg/ms)
μ_t	Eddy or turbulent viscosity (kg/ms)
μ^*_t	Dimensionless eddy or turbulent viscosity *($\mu^*_t=\mu_t/\mu$)*
ν	Kinematic viscosity (m^2/s)
ν_t	Turbulent kinematic viscosity (m^2/s)
ρ	Density (kg/m^3)
σ_k , σ_t , σ_ω	Prandtl numbers for turbulence kinetic energy, temperature and dissipation of turbulence kinetic energy, respectively
τ	Dimensionless time
ω	Specific dissipation rate of kinetic energy (m^2/s^3)
ω^*	Dimensionless specific dissipation rate of ($\omega^* = \omega H/\sqrt{g\beta\Delta TH}$)

Appendix I

Flow Chart of the Computer Program